ACS NANO

Cite This: ACS Nano XXXX, XXX, XXX−XXX

www.acsnano.org

ARTICLE

On-Chip Stretching, Sorting, and Electro-Optical Nanopore Sensing of Ultralong Human Genomic DNA

Adam Zrehen,[†] Diana Huttner,[†] and Amit Meller*[,†,‡]

[†]Department of Biomedical Engineering, Technion − IIT, Haifa 32000, Israel

[‡]Russell Berrie Nanotechnology Institute, Technion − IIT, Haifa 32000, Israel

Supporting Information

ABSTRACT: **Solid-state nanopore sensing of ultralong genomic DNA molecules has remained challenging, as the DNA must be controllably delivered by its leading end for efficient entry into the nanopore. Herein, we introduce a nanopore sensor device designed for electro-optical detection and sorting of ultralong (300+ kilobase pair) genomic DNA. The fluidic device, fabricated in-silicon and anodically bonded to glass, uses pressure-induced flow and an embedded pillar array for controllable DNA stretching and delivery. Extremely low concentrations (50 fM) and sample volumes (~1 μL) of DNA can be processed. The low height profile of the device permits high numerical aperture, high magnification imaging of DNA molecules, which remain in focus over extended distances. We demonstrate selective DNA sorting based on sequence-specific nick translation labeling and imaging at high camera frame rates. Nanopores are fabricated directly in the assembled device by laser etching. We show that uncoiling and stretching of the ultralong DNA molecules permits efficient nanopore capture and threading, which is simultaneously and synchronously imaged and electrically measured. Furthermore, our technique provides key insights into the translocation behavior of ultralong DNA and promotes the development of all-in-one micro/nanofluidic platforms for nanopore sensing of biomolecules.**

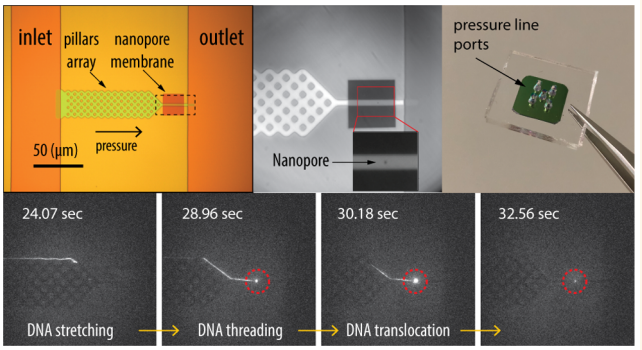

KEYWORDS: *solid-state nanopore, electro-optical sensing, genomic DNA, single-molecule sensing, nanofluidics, microfluidics*

Analysis of long genomic DNA (gDNA), *i.e.*, >100 kilobase pair (kbp), can facilitate mapping of large-scale genomic alterations, including transpositions, inversions, segmental duplications and copy number variations,[1,2] which is currently a challenge for DNA sequencing methods, particularly Next Generation Sequencing (NGS).[3] The manipulation and sensing of long individual gDNA molecules require sophisticated means to uncoil and stretch individual DNA polymers without shearing them while permitting sensing of the relevant information. Another outstanding challenge is how to target or enrich specific DNA fragments from the whole genome; single-molecule analysis methods are inherently limited in their throughput, hence lowering the probability of probing the fragments of interest. To date, methods such as DNA combing[4,5] and nanochannels[6−8] have been developed for this purpose, providing useful biomedical information and in some cases disease relevant data, which is difficult to obtain using NGS. While these methods are efficient at mapping large-scale genomic motifs and producing genome-specific DNA barcodes,[9,10] they are subject to optical resolution limits. Consequently, the development of complementary sensing modalities that can sort and uncoil long DNA may expand the range of possible gDNA-based applications.

Nanopores have recently emerged as a powerful single-molecule sensing method and consequently have been adapted for a broad range of biosensing applications including purely electrical DNA sequencing, genotyping and methylation quantification.[11−13] In particular, solid-state nanopores (ssNPs), considered to have superior properties in terms of manufacturability and electro-mechanical robustness over protein pores,[11] have been shown to be efficient as genotyping tools as well as for mapping the interactions of bound proteins such as transcription factors or other proteins such as RecA to DNA.[14,15] Nevertheless, to date ssNP sensing has involved substantial off-chip biochemical preparations, and in some

Received: October 6, 2019
Accepted: November 22, 2019
Published: November 22, 2019

DOI: 10.1021/acsnano.9b07873
ACS Nano XXXX, XXX, XXX−XXX

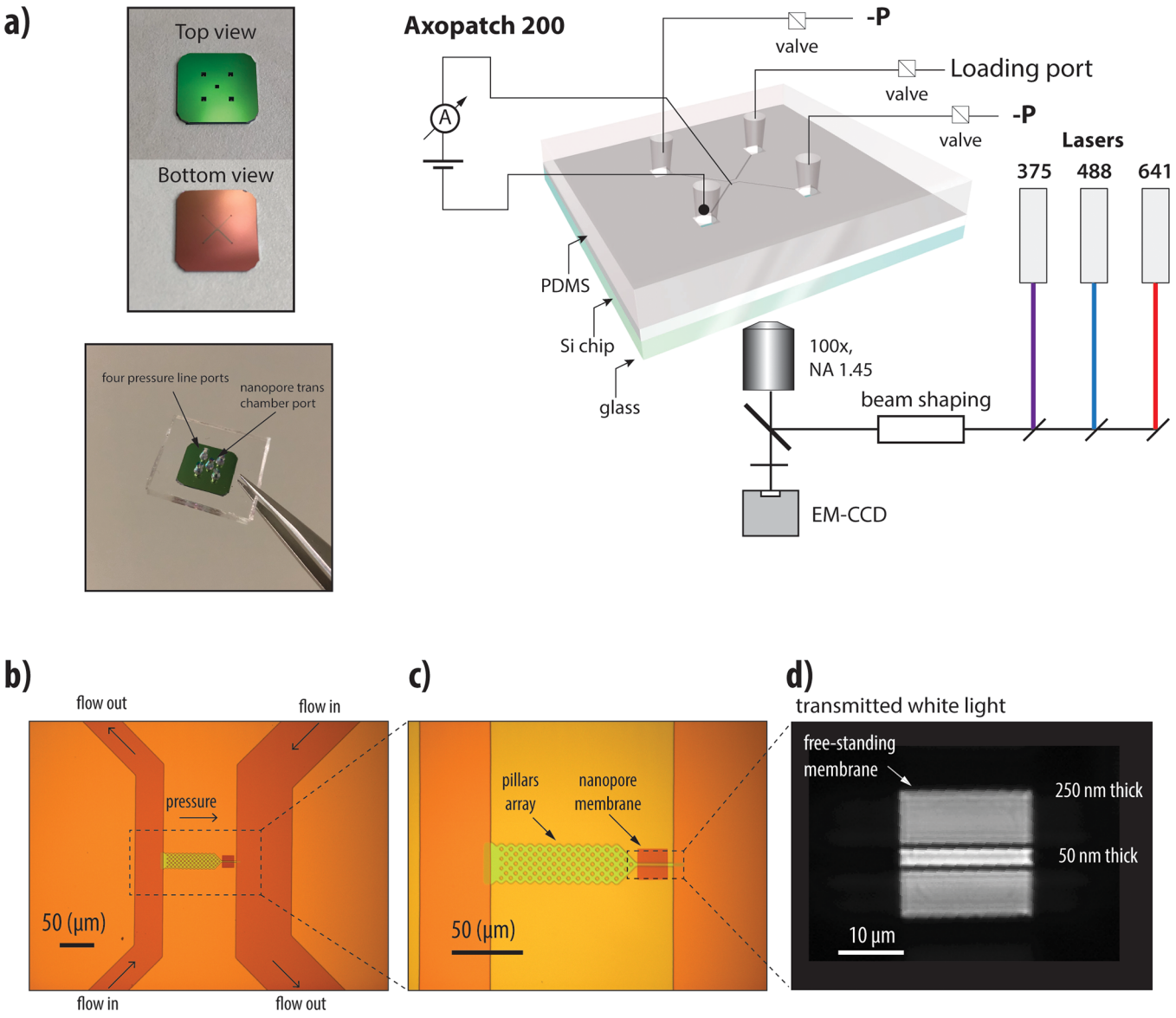

Figure 1. Fluidic pillar array for DNA stretching and sorting integrated with a nanopore for electro-optical single-molecule sensing. (a) Right: Illustration of Si chip sealed by glass and bonded to PDMS for access ports. Bottom leftmost image shows actual device. The optical setup consists of three lasers: 488 and 641 nm for wide-field excitation of fluorescently labeled DNA molecules and 375 nm for nanopore fabrication by laser-etching. Top leftmost image shows top and bottom views of the chip before anodic bonding to glass and plasma bonding to PDMS. (b) Bright-field 20× image of device showing microchannels bridged by the pillar array. DNA is driven in the direction of the pressure gradient. (c) 50× image of the pillar array connecting to a narrow channel situated atop a free-standing membrane. (d) Transmitted white light image of the free-standing membrane bisected by a ∼2.5 μm 200 nm deep channel in which a single nanopore is fabricated.

cases amplification of the target DNA sequence. Furthermore, absent a motor enzyme,[16] ssNP sensing of ultralong unamplified gDNA has remained challenging, as the DNA must be controllably delivered and uncoiled immediately before it is fed to the nanopore. Failing to bring the DNA's end to the proximity of the pore may result in loss of the molecule, irreversible clogging, and an extremely low capture rate probability.[17−20]

In addition to the need to develop sophisticated means for manipulation of ultralong DNA, the rise of point-of-care diagnostics has significantly fueled the development of nanopore sensors with additional on-chip functionality, specifically for whole genome processing. To that end, nanopore sensors have been integrated with microchannels[21,22] or microvalves for fluid handling,[23] as well as containment chambers for reactions and purification.[24] Besides methods for bulk handling of DNA, researchers have investigated the controlled delivery of single DNA molecules to the nanopore. For example, Zhang *et al.* embedded a nanopore within a nanochannel and captured a fluorescently labeled λ DNA molecule, albeit, without any electrical sensing.[25] More recently, a two-pore device was assembled for trapping a single DNA molecule in a "tug of war" between the pores.[26,27] Nonetheless, most practical applications of the sensor have treated DNA preparation and sensing as separate steps, relying on purified and amplified DNA samples up to just a few tens of kilobase pairs in length.

Nanopore biosensing requires low-noise and high-bandwidth electrical measurement of ion flow through a unitary pore having comparable dimensions to the molecule's cross-

DOI: 10.1021/acsnano.9b07873
ACS Nano XXXX, XXX, XXX−XXX

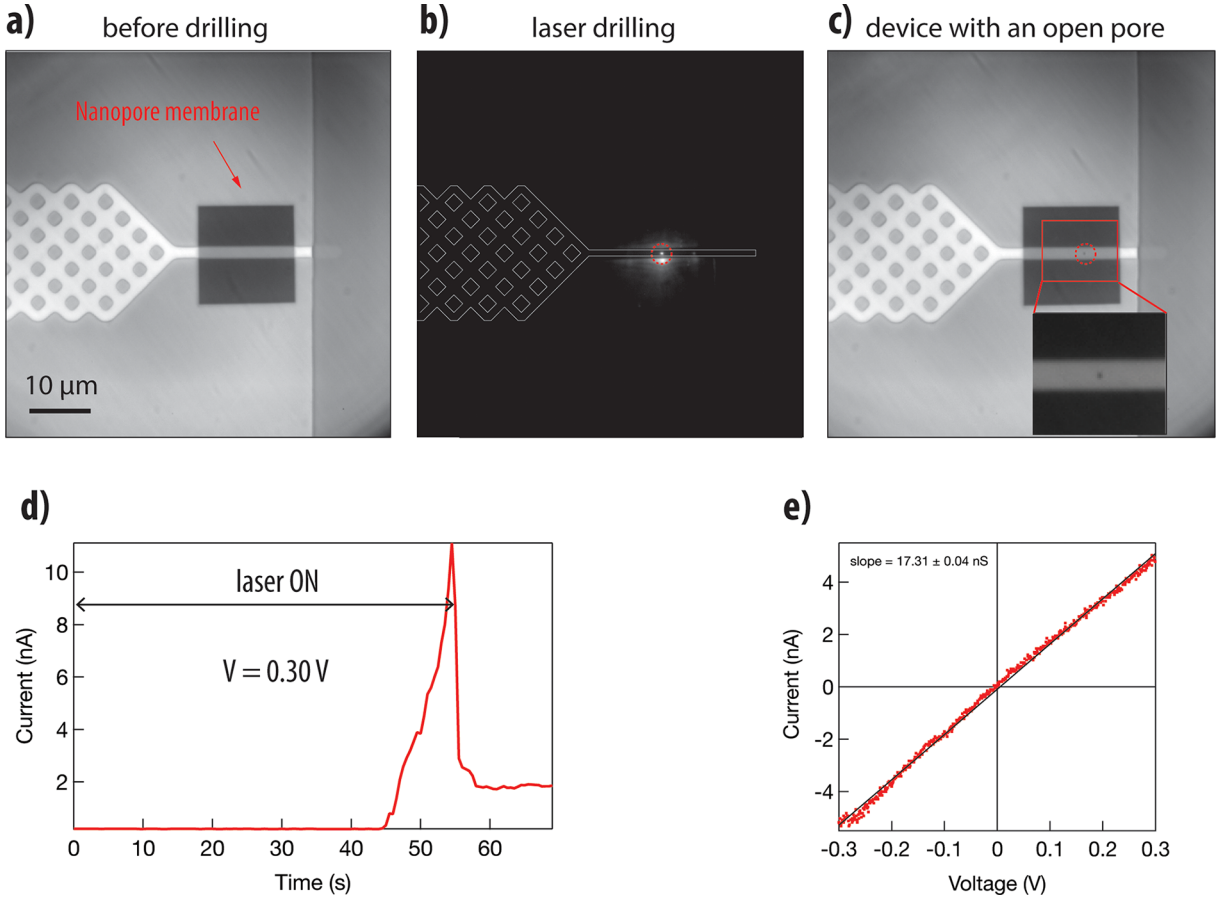

Figure 2. ***In situ*** **laser drilling of a nanopore in a fluidic channel. (a) 100× image of the free-standing membrane before drilling a nanopore within the ~2.5 μm 200 nm deep channel. (b) Laser-drilling process showing photoluminescence emitted by the confocal laser focus at the fabrication site. (c) Free-standing membrane after drilling is altered by a thin darker region at the nanopore position. (d) Ionic current measured at 300 mV during laser-etching with a ~ 15 mW 375 nm laser in 1 M KCl pH 10. Nanopore formation is signaled by a rise in current and occurs at roughly 45 s. (e) Current−voltage measurement in 1 M KCl following pore stabilization (conductivity, σ ~ 17 nS).**

section. This has been achieved by the fabrication of an ultrathin, freestanding, insulating membrane such as Si-rich silicon nitride, in which typically sub-20 nm nanopores are formed. However, the integration of such sensors with a virtually planar fluidic device compatible with high magnification and high-resolution single-molecule fluorescent imaging has remained cumbersome due to the strict requirements imposed by high numerical aperture optics (short working distance) and low capacitance noise (high bandwidth electronics). Herein, we present a monolithic nanopore sensor device that uses an interfaced pillar array and controllable pressure-induced flow for single-molecule delivery. Our device can uncoil gDNA fragments over 400 kbp in length, which are extracted from human cancer cells and fluorescently labeled, feeding them one by one into the integrated nanopore for analysis. Instead of relying on soft-lithography microfluidics (*i.e.*, polydimethylsiloxane, PDMS, casting), we implemented a complete in-silicon design permanently fused to glass for high-resolution feature formation, enabling high magnification (100x objective) multicolor single-molecule fluorescence imaging. We show that DNA molecules can be sorted prior to the stretching stage based on sequence-specific fluorescent tags, permitting precise targeting of the desired DNA for efficient sampling. Optical sorting prior to nanopore analysis sharply decreases the effective target DNA concentration down to a few tens of femtomolar (10^{-15} M). Furthermore, the chip design enables high magnification imaging of single translocation events synchronized to the electrical signal, providing insights on nanopore translocation behavior.

RESULTS AND DISCUSSION

Design and Fabrication. The design features a central silicon nitride pillar array, as is commonly used for stretching ultralong DNA molecules,[28,29] and a narrow channel (~2.5 μm wide and 200 nm deep) for funneling linearized molecules to the nanopore. The entire device is sealed by thin (150 ± 8 μm) borosilicate glass to enable high resolution (100×, NA = 1.45) observation of single molecules during sorting, stretching, and in the proximity of the nanopore. The shallow depth of the narrow channel also ensures that DNA molecules always fall within the nanopore capture radius. Microchannels in an easy-to-flush U-shape are connected by through-holes etched through the silicon substrate to four liquid reservoirs made in a thick PDMS slab bonded to the silicon substrate on the back side (Figure 1a). A single port on each side of the chip accepts plastic tubing for applying negative pressure. The final port on the entry side can be loaded with sample to be pulled into the microchannel by pressure flow. The U-shaped microchannels are bridged by a narrower channel containing the pillar array, leading to a finer passage that is situated atop a free-standing silicon nitride (SiN_x) membrane in which a single nanopore is fabricated (Figure 1b−d). A fifth reservoir

DOI: 10.1021/acsnano.9b07873
ACS Nano XXXX, XXX, XXX−XXX

connects to the *trans* side of the membrane and accepts an AgCl electrode for applying positive bias referenced to a *cis* electrode on the outlet side of the pillars. While the microchannels on both sides are the same depth (~650 nm), the entry-side channel is half the size of the outlet-side channel in order to restrict all passing molecules to within the field of view of the camera. The outlet-side channel, 100 μm in width, is made larger to minimize the ohmic resistance between the *cis* and *trans* electrodes and thus maximize the nanopore signal.

Device Sealing by Anodic Bonding. While the literature on glass bonding to silicon and silicon dioxide (SiO_2) is extensive, there are fewer examples of glass bonding to SiN_x. Moreover, given the fragility of the thin free-standing membrane, our initial attempts to bond glass to SiN_x used thin spun-on coatings such as sodium silicate[30] and polysilsesquioxane,[31] which would not expose the chip to high temperatures or stresses for prolonged periods. However, these coatings rely on condensation reactions between the silanol groups of the glass and the substrate, and SiN_x has a low density of silanols. Hence, we failed to achieve uniform and reproducible bonding over the surface of the chip. As an alternative, we tried a low temperature anodic bonding method developed specifically for SiN_x,[32] which was shown to form strong bonds in as little as 15 min, significantly faster than low temperature annealing on its own.[33] For anodic bonding to work, it was necessary to form a thin $SiO_2/Si_xO_yN_z$ layer on the SiN_x surface by subjecting it to oxygen plasma. Importantly, the plasma power was kept low (25 W) to minimize surface roughening which can inhibit the bonding process, as described by Weichel *et al.*[32] Anodic bonding optimization was carried out between 400 and 1000 V on a 350−400 °C hot plate for 10−90 min with borosilicate glass (Borofloat 33), which has a matching thermal expansion coefficient to SiN_x.

At these bonding conditions, it was necessary to preserve the 500 nm thick SiO_2 layer as structural support for the SiN_x membrane to prevent membrane deflection and bonding to the glass. This behavior was also observed with the oxide layer in place when the aspect ratio of the channel exceeded roughly 15 (depth = 200 nm, width = 3 μm). Membrane collapse was observable as a contrasted area in a white light microscope or by imaging Alexa Fluor 488 in the channel, as shown in Figure S2 for various designs. In accordance with an expected V^2t_{end} likelihood of contact,[34] where V is the applied voltage and t_{end} is the total bond time, we found that bonding could be accelerated by applying a high voltage (1000 V) for a short period of time (14 min). Minimizing the quotient V^2t_{end} was critical to prevent excessive membrane strain and cracking, which showed up as a leakage through the membrane after oxide removal.

Nanopore Fabrication by Laser-Etching. Given the high temperature and stresses induced by anodic bonding, it was crucial to find a nanopore fabrication method that could be done *in situ*, after the device was sealed by glass. While dielectric breakdown only requires electrolytic contact of the two surfaces of the membrane and could thus be used to form a pore in a sealed device,[35,36] nanopore formation is not easily localized.[37,38] To control the nanopore position requires selective thinning of the membrane by an upstream lithographic and RIE process, which is challenging to align in a ~2.5 μm channel. Hence, we opted for a recently developed nanopore fabrication technique based on laser-etching, which offers diffraction-limited (~200 nm) control of the nanopore position.[39,40] These studies showed that the laser-drilling process is highly sensitive to the material Si content, buffer pH, and laser wavelength. Taking advantage of these findings, we used a near-ultraviolet laser (375 nm, 10−15 mW) to form a nanopore precisely located at the center of the narrow channel. Parts a and c of Figure 2 show the channel area and the SiN_x free-standing membrane before and after laser irradiation, respectively (reflected white light illumination), and during laser drilling (Figure 2b). A darker (thinner) spot is clearly observed following laser illumination. Figure 2d and Figure S4 present example current traces for the etching process leading to nanopore formation, signaled by a rise in current above the baseline value. Etching occurred in 1 M KCl pH 10, and nanopores were typically formed within 50 s based on over 40 trials (see Table S1 for a summary of tested devices). Subsequently, the nanopore was allowed to stabilize over a few minutes, and the $I-V$ response was measured, as shown in Figure 2e. Based on the pore conductance obtained from the slope, and taking into consideration the channel resistance (6.0 ± 0.2 MΩ), we estimated this particular pore to be 4.5 ± 0.5 nm in diameter for an effective thickness range of 4−6 nm as predicted by Gilboa et al.[39] Nanopores can be subsequently expanded by laser or by applying moderate voltage pulses (1−5 V).

Selective Uncoiling and Stretching of Long gDNA. To date, DNA translocation measurements through solid-state nanopores have been limited to short or medium length DNA, typically up to ~48.5 or 97 kbp (*i.e.*, λ phage genome monomer or dimers).[41,42] Moreover, most nanopore studies use either synthetic DNA (*i.e.*, PCR replica of the target DNA) or plasmids amplified in host bacteria. Consequently, little is known about the propensity of much longer DNA (*i.e.*, > 100 kbp) to enter pores. In particular, the rate at which DNA (as well as other charged molecules) are captured by the pore is governed by the size of the capture radius around the pore in which molecules are electrically attracted. In bulk solution, double-stranded DNA (dsDNA) forms Gaussian coils, which are well approximated by a wormlike chain model for which the root mean-square end-to-end distance is $\sqrt{R^2} = \sqrt{2PL_0}$, where P is the persistence length (about 50 nm) and L_0 is the contour length. In the case of ultralong DNA, the coil size may exceed the capture radius of the nanopore, hence raising a question about its capture rate and capture probability.[42] The problem is compounded by the potential for DNA clogging, which may occur depending on the molecule's initial configuration. Uncoiling and stretching the dsDNA and physically bringing one of the DNA ends to the pore vicinity may therefore be a prerequisite to efficient DNA capture and avoiding irreversible clogging.

We first quantified the extent by which the device can stretch and disentangle ultralong DNA. While short (*i.e.*, tens of kbp) strands are commonly isolated from cells with the aid of centrifugation, extraction and preservation of ultralong gDNA fragment requires a more delicate procedure: To prevent DNA fragmentation, human cancer cells were encapsulated in agar plugs for controlled cell lysis and DNA release (see the Supporting Information). The agar was subsequently enzymatically digested, and the DNA molecules were stained for high-resolution imaging using the intercalator dye YOYO-1 (see the Materials and Methods) which is known to induce molecule extension of around 5% for our staining ratio of 1:20 (bp:dye) and assuming a linear dependence on

DOI: 10.1021/acsnano.9b07873
ACS Nano XXXX, XXX, XXX−XXX

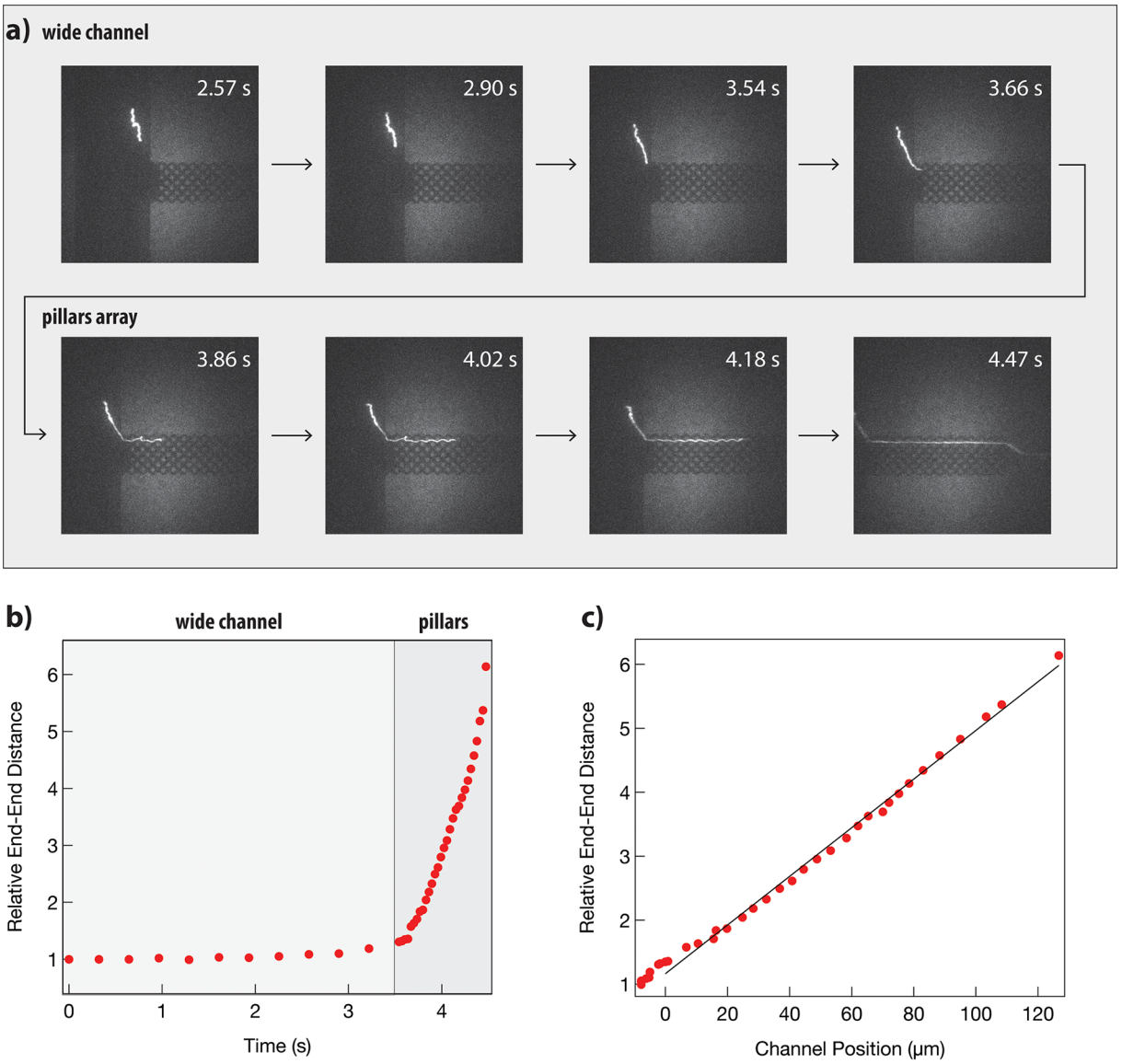

Figure 3. Ultralong genomic DNA uncoiling and stretching in a pillar array. (a) YOYO-1 labeled DNA (20:1 bp:dye) in TE buffer is pulled by 8−10 mbar vacuum from the ∼650 nm deep microchannel through the 200 nm deep pillar array over 4.5 s. (b) End-to-end distance of the DNA strand relative to its starting end-to-end distance in the microchannel as a function of time. The end-to-end distance increases about 6-fold for this molecule for a contour length of ∼140 μm or at least 390 kbp (adjusted for YOYO-1 extension by 5%). (c) End-to-end distance of the DNA strand increases linearly with the position in the pillar array.

YOYO-1 concentration.[43] The DNA molecules were first loaded by applying a negative pressure of ∼990 mbar across the ∼650 μm in depth microchannel, resulting in partial elongation due to the constriction of the microchannel and the pressure-induced flow. The molecules were subsequently imaged at high-speed (∼30 FPS) and high magnification (60× or 100× objectives) as they were forced through the nanopillar array.

The transition from the deep microchannels to the pillar region (∼200 nm deep) presents an entropic barrier to DNA coil migration and results in substantial elongation of the molecule, as observable in Figure 3a (see also Supporting Movie S1). The DNA strands are further disentangled and elongated at the pillar array, which acts as a molecular sieve, due to the increased fluid velocity (due to lower area) and hooking/unhooking to the pillars.[44] Rather than achieving complete DNA linearization, our goal was to sufficiently uncoil the DNA in order to expose one of its ends to the pore proximity; hence, the pillar design was loosely derived from literature examples[6,29] as well as experimentation with designs of different pitch and pillar diameter. Generally, we found that smaller pillars (*e.g.*, 2 μm compared to 4 μm) and a smaller pitch (*e.g.*, 2 μm compared to 3 μm) were more effective at hooking DNA, resulting in uncoiling and semilinearization of strands beyond the camera field of view (136 μm). Additional examples of DNA stretching, particularly highlighting hooking/unhooking to the pillars, are given in Figure S6.

We estimated the end-to-end distance of a partially stretched representative DNA molecules as a function of time and position, before and after entering the pillar array (Figure 3b,c). Upon entering the pillar array, the dsDNA sharply stretches, which appears to be roughly linear with the extent to which the DNA traverses the pillars and reaches at least 6-fold (Figure 3c) along a 120 μm travel distance. Importantly. This

DOI: 10.1021/acsnano.9b07873
ACS Nano XXXX, XXX, XXX−XXX

stretching "exposes" a DNA end, positioning it in the proximity of the nanopore's capture radius, which has been optimized to extend 15−30 μm laterally toward the pillars, as discussed in a later section.

DNA Sorting. Genomic DNA samples as well as other biological DNA samples from clinical sources contain a wide range of DNA fragment lengths and types. In many practical cases, the target DNA will constitute only a small fraction of the total DNA, hence presenting a challenge for nanopore sensing and analysis. In particular, when processing thousands of long DNA molecules, nanopores may clog before sufficient sampling of the target DNA. Preselection strategies used to enrich the desired DNA population may therefore be essential for successful sensing. Unlike conventional nanopore sensors where samples are sensed indiscriminately, our microfluidic platform enables selective sampling, in addition to rapid buffer and sample exchange. As such, DNA molecules that are entangled with one another or too short can be forced to bypass the pore. Alternatively, multicolor and sequence-specific DNA labeling can be used for more efficient sensing. To demonstrate this principle, DNA was prepared by nick translation using site-specific nicking enzyme Nt.BspQI and by Taq polymerase incorporation of Atto-647N, followed by YOYO-1-labeling of the backbone. The Nt.BspQI enzyme was chosen due to its proven efficiency and sequence selectivity, but it should be noted that other labeling methods could be employed targeting different recognition sequences (*e.g.*, CRISPR-CAS9 nickase labeling[45]) or epigenetic modifications (*e.g.*, 5-hmC labeling[8]). Incorporation of the Atto dye occurs on average every 10−15 kbp, as determined by image analysis of DNA molecules stretched on glass (Figure 4a and Figure S3).

For DNA sorting, we developed a labeling scheme whereby molecules are either one or two color labeled: DNA molecules that are labeled by nick translation (the Atto647N dyes) constitute the majority of the sample and are allowed to flow past the nanopillar array. In contrast, molecules not labeled by nick translation trigger opening of the electrically actuated pressure valve, stopping them at the pillar entrance for subsequent stretching and nanopore sensing (done manually). The silicon dioxide microchannels have low photoluminescence in the 400−750 nm range and, given their shallow depth (~650 nm), passing molecules are either in focus or slightly out of focus but still distinguishable as either one or two color labeled. Hence, selection can be made upstream of nanopore sensing in the faster moving microchannel (600−700 μm/s), which is useful when the molecule of interest is rare, requiring sifting through hundreds or even thousands of molecules during which the nanopore can irreversibly clog. In Figure 4b, we focus on two typical DNA molecules out of thousands not shown. The molecules are imaged using an EMCCD at high speed (~30 FPS) for fast software-based decision-making. This trigger mechanism is also employed (along with manual control) for stopping DNA at the pillar exit, as shown in Supporting Movie S2.

To evaluate the sampling efficiency, we quantified the molecule delivery rate to the pillars as a function of concentration. For this we used shorter YOYO-1-labeled DNA strands of a uniform length (10 kbp) that would not shear and hence whose concentration can be determined accurately in bulk using a UV−vis spectrometer. As depicted in Figure 4c, in the range of nearly 3 decades in concentration from 50 fM to 10 pM, the molecule delivery rate to the pillars

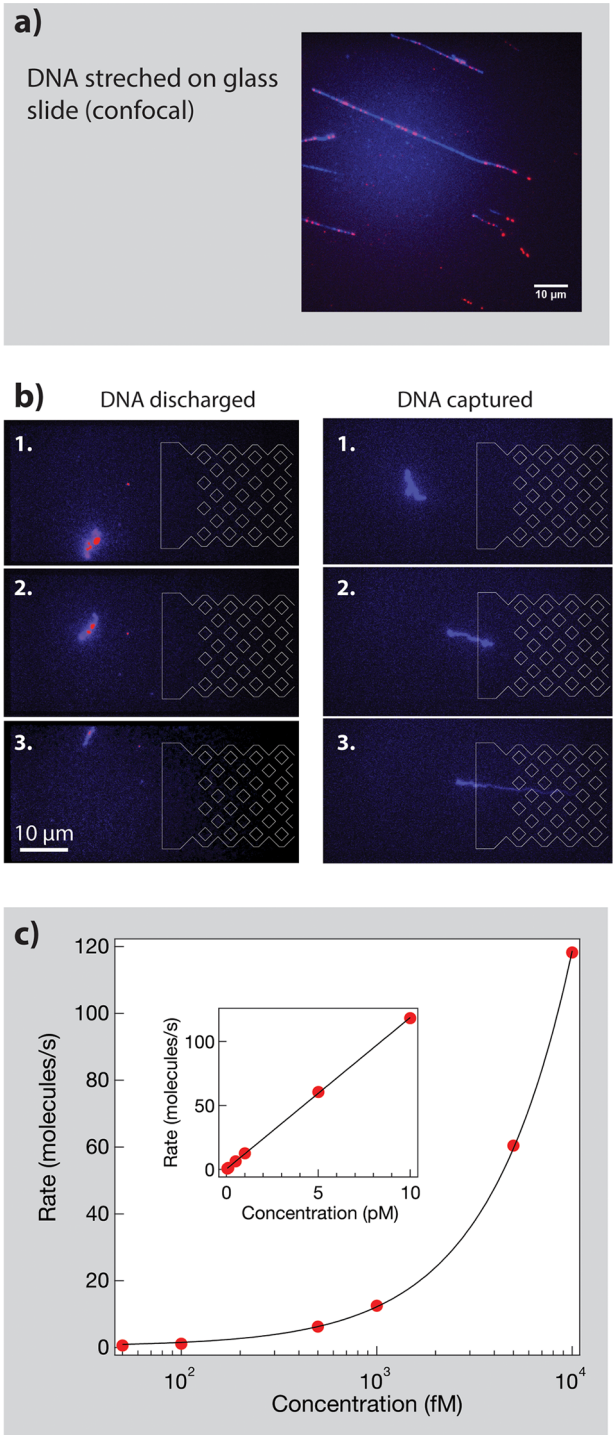

Figure 4. DNA sorting based on sequence-specific fluorescent tags. (a) DNA stretched on glass that has been nick-translated with site-specific Nt.BspQI for Atto647N labeling in red and subsequently labeled with a YOYO-1 backbone in blue. (b) Principal and implementation of two-color fluorescence sorting. Molecules labeled in both red and blue are vacuumed past the pillar array, whereas the blue-only molecules are stopped at the pillar array for subsequent stretching and delivery to the nanopore for sensing. (c) Delivery rate of YOYO-1 labeled 10 kbp dsDNA to the pillar as a function of DNA concentration (measured in a single device).

varies from ~0.65 to 120 s^{-1}. In Figure 4c (inset) we show that the dependence of the capture rate on concentration is linear, as expected, implying that the yield remains constant across

DOI: 10.1021/acsnano.9b07873
ACS Nano XXXX, XXX, XXX−XXX

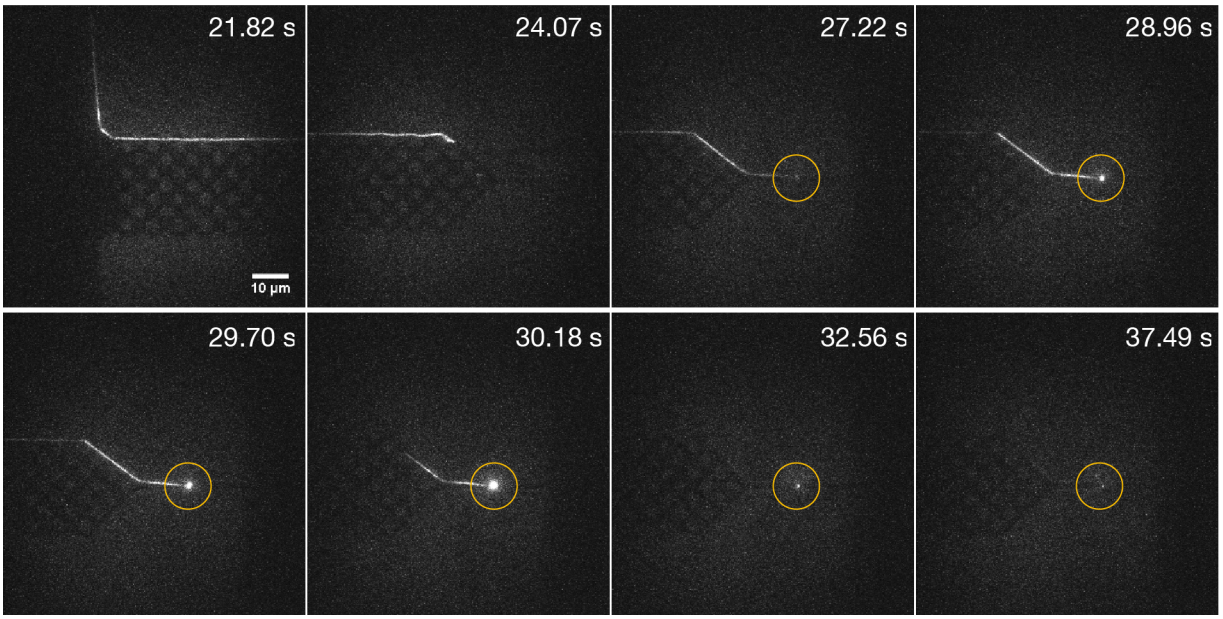

Figure 5. Translocation of ultralong DNA. YOYO-1-labeled DNA is delivered to the nanopore by vacuum and subsequently electrophoretically driven through a ~20 nm nanopore at a 1 V applied bias. The first image (21.82 s) shows the DNA traversing the pillar array, already uncoiled. At 24.07 s, the vacuum is shut off, at which point the DNA is pulled to the nanopore (indicated by a yellow circle), making contact at 27.22 s. It then translocates for the next several seconds, and by 30.18 s, the lagging strand of the DNA becomes visible. By 32.56 s, the DNA has mainly disappeared to the other side of the membrane, and the nanopore is ready to accept a new molecule (37.49 s).

this concentration range. Notably, extremely low concentrations of starting material can be used with high capture rate to the nanopillar array region. Similarly, the sample loading volume is comparatively small (~1 μL fills the PDMS loading port), making our device highly compatible with clinical DNA samples.

Nanopore Capture and Translocations. While the YOYO-1-labeling strategy employed here served for a convenient proof of principle, which could in theory be substituted by covalent labeling, it was necessary to load the DNA at low salt (<100 mM) to prevent rapid YOYO-1 unbinding.[46] However, the *cis* electrode, placed at the pillar exit, could be filled with higher salt concentrations. As the electrode is placed on the opposite side of DNA movement, the electric field lines around the pore are somewhat biased away from the DNA; however, by applying a salt gradient across the nanopore, as implemented in a conventional nanopore sensor,[42] we were able to extend the capture radius significantly. In particular, we used a 1:10 salt gradient (0.1:1 M KCl *cis*/*trans*. The effect is that the DNA is immediately pulled toward the pore after being delivered within 20−30 μm and the vacuum is shut off. Since the device depth at this stage is only ~200 nm, the molecule's position with respect to the membrane surface has negligible impact on capture. To ensure sufficient nanopore signal strength, we used high voltages (500−1000 mV), and typically nanopores up to 20 nm exhibited a detectable signal. The nanopore noise was between 50 and 70 pA RMS at 10 kHz with the blue widefield laser off and 100−200 pA with the laser on at ~5 W/cm^2 (see Figure S5 for the noise spectrum).

We first examined the translocation of ultralong DNA through larger (*i.e.*, 15+ nm) pores suitable for the detection of transcription factors, DNA binding proteins, or other bound targets. To accurately determine the point at which the DNA engages and exits the nanopore, we performed these and other translocation experiments at 100×. Figure 5 and Supporting Movie S3 present an example translocation event in a 20 nm pore, in which a minimum 400 kbp strand is translocated (*i.e.*, the event is so long that we have given a conservative estimate based on the 100× image and translocation duration). At 24.07 s, the vacuum is turned off, and the DNA is immediately electrophoretically pulled to the pore, making contact at 27.22 s. The DNA is subsequently pulled through over the next 2.96 s, and by frame 30.18, the DNA is still translocating. A visible fluorescent spot remains over the next 2−3 s. As the lagging strand will be pulled to the pore independent of whether the leading strand has translocated, it appears the DNA accumulated somewhat at the pore mouth, and by 32.56 s, has mainly disappeared to the other side of the pore. For this particularly long event and large nanopore, we could only discern a distinct electrical signal at the DNA entry into the pore (~300 pA drop).

In Figure S7 we analyzed the DNA molecule speed before, during, and at the end of translocation. During the capture phase, the DNA accelerates from rest to about 19 μm/s, at which point it contacts the nanopore and accelerates. At around 28.9 s, the appearance of a distinct ~4 μm (~15 kbp) segment with low YOYO-1 labeling density provides us a means of directly measuring the translocation speed, for which we obtain ~130 μm/s, roughly constant over 8 frames. It is well-established that partially denatured AT-rich regions present as dark patches in YOYO-1 denaturation mapping assays, and hence, the observed dark segment is likely an AT-rich region with a low melting point (at our given salt concentration).[47,48] Nearing the end of the translocation, the DNA speed through the pore increases 3-fold (390 μm/s) and reaches at least 800 μm/s for the remaining ~26 μm of threading. The optical translocation profile suggests that early in the threading process, there is a large drag force on the

DOI: 10.1021/acsnano.9b07873
ACS Nano XXXX, XXX, XXX−XXX

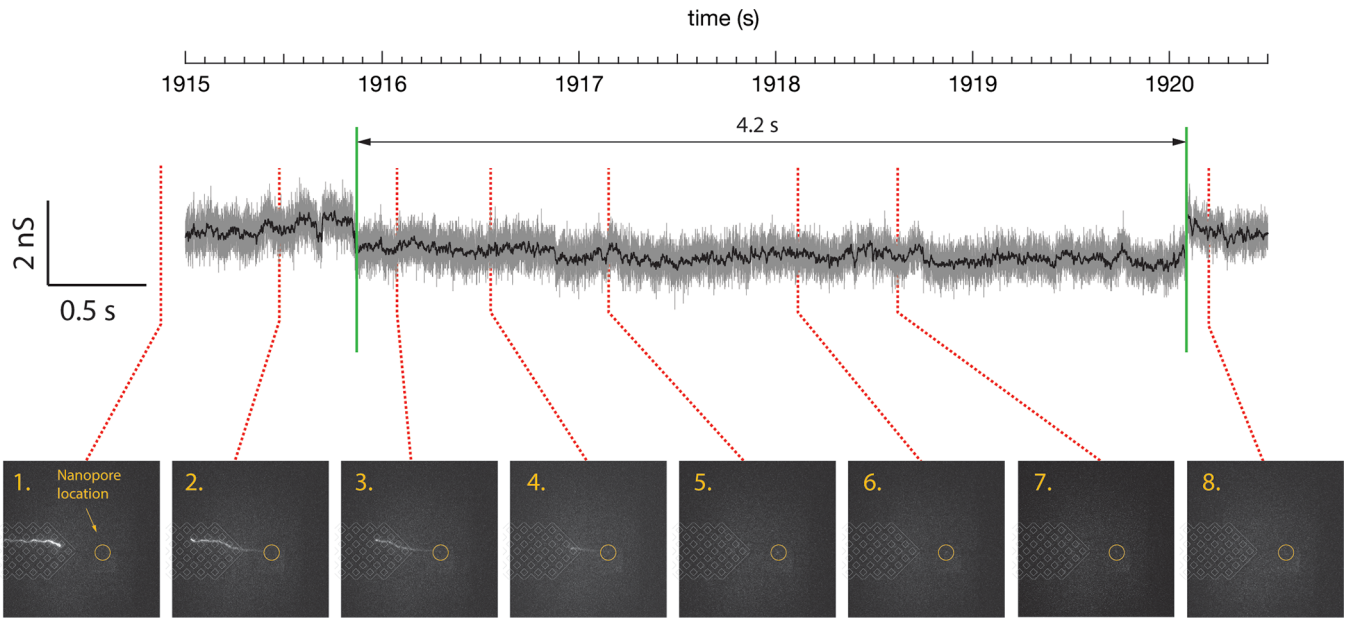

Figure 6. Electro-optical translocation of ultralong DNA. Top shows the electrical recording through a 12 nm nanopore at a 1 V applied bias (gray trace, 10 kHz; black trace, 1 kHz) during which a ~60 μm in contour length YOYO-1-labeled double-stranded DNA is translocated. The electrical event is aligned to a series of images (1−8) taken at 100× using an EMCCD at 25 ms exposure, showing the YOYO-1-labeled DNA before and during translocation. At frame 1, the vacuum has been shutoff, resulting in an electrophoretic migration to the pore. The DNA subsequently translocates and exits the nanopore over the subsequent frames (2−8). The conductance drop associated with DNA threading is indicated by the two green vertical lines.

ultralong molecule causing it to thread slowly compared to when the bulk of the molecule has passed through the pore.

We also electrically recorded translocations of long DNA molecules in smaller pores (<15 nm). Figure 6 depicts such a sequence in which the nanopore current and EMCCD video are simultaneously and synchronously recorded (see also Supporting Movie S4): In the first snapshot, the DNA molecule has uncoiled and stretched and is within close enough proximity to the nanopore such that terminating the vacuum (second snapshot) results in an electrophoretic migration toward the pore, as in the larger pore described above. Around 1915.9 s, the DNA end engages the nanopore (third snapshot), resulting in a sharp downward transition in nanopore conductance (green vertical line). The amplitude of the conductance drop is proportional to the surface area of an unfolded dsDNA molecule in the nanopore (d = 12 nm). Following this transition, we literally observe the translocation of the DNA through the nanopore, as the YOYO-1 rapidly dissociates from the DNA in the higher salt *trans* chamber leaving only a weak fluorescence spot at the nanopore location (yellow circle). Around 1920.1 s the nanopore conductance restores to its open level, again in an abrupt transition (2nd green line), at which point the nanopore is ready to accept another DNA molecule.

Based on the stretched image of the DNA, we approximate its contour length as about 60 μm (assuming our device can achieve about 80% stretching of the molecule, as described in the Supporting Information). Therefore, the 4.2 s translocation time corresponds to a rate of about 23 μs/bp. Notably, this amounts to >3 orders of magnitude slowing down compared with previous DNA translocation studies using comparable nanopores at 1 V bias. The translocation time is significantly longer for larger pores as well (*i.e.*, 20 nm), as presented earlier, in which the 300+ kbp strand takes over 3 s to fully clear the pore. The last two frames (60 ms) show a clearance of about 100 kbp or ~0.5 μs/bp based on the migration of the DNA lagging strand to the pore. At a YOYO-1 staining ratio of 1:20 (bp:dye), the molecule's effective negative charge only reduces to 90%. Therefore, the slow translocation is likely attributable to the orientation of DNA entry with respect to the electric field lines or a larger drag force imparted on the ultralong molecule.

CONCLUSIONS

In this work, we presented the fabrication and implementation of a fluidic device for controlled single-molecule delivery and nanopore sensing of ultralong genomic DNA. As an in-silicon design anodically fused to glass, the device is compatible with high-magnification (100× high NA objective) multicolor fluorescent imaging. For nanopore fabrication, we utilized a recently developed laser-etching technique, showing its advantages over conventional methods (*e.g.*, TEM, dielectric breakdown) for *in situ* localized nanopore formation. By using fast-moving pressure-induced flow, DNA concentrations as low as 50 fM, as may be expressed in rare samples, can be readily delivered to the nanopore for sensing. Further gains in sampling efficiency are made possible by multicolor fluorescent labeling of the DNA molecules, as we presented preliminarily. Next, we demonstrated the translocation of ultralong DNA (>300 kbp) through 10−20 nm nanopores, suitable for electrical detection of bound protein targets such as RecA or other DNA binding proteins. While this work focused on YOYO-1 labeling, alternative fluorescence labeling strategies may be applied, such as BrdU/EdU, as is common for investigating DNA replication. In particular, the use of covalently attached fluorophores may permit DNA resensing, which in combination with the observed slow translocation time (~20−25 μs/bp), presents a possible avenue for DNA sequencing and will be the subject of further study. In addition to the practical applications discussed here, direct visualization

DOI: 10.1021/acsnano.9b07873
ACS Nano XXXX, XXX, XXX−XXX

of DNA translocation behavior (*e.g.*, failed entries, Figure S8) may complement our existing understanding of DNA translocation dynamics,[49] hitherto dependent primarily on electrical data and theoretical modeling.

MATERIALS AND METHODS

Chip Fabrication. Fabrication began by depositing 200 nm of low stress SiN_x onto a starting $SiN_x/SiO_2/Si$ wafer (50 nm/350 nm/350 μm) by PECVD (300 °C) in order to increase the workable channel depth. Following cleaning in solvents (acetone, methanol, 2-propanol, water), the wafer was baked on a hot plate at 300 °C for 10 min. AZ1518 resist was spin-coated at 4000 rpm to a thickness of ∼1.8 μm and baked on a hot plate at 120 °C for 2 min. The pillar structures were exposed by UV light (MicroWriter ML3), developed in Novo Developer (2.14% TMAH in water), and subsequently etched by reactive ion etching (RIE) with 10 sccm CF_4 and 10 sccm O_2 (75 W, 0.15 mbar). Microchannels were then front side aligned to the pillars and etched by RIE through the entire SiN_x thickness. The ∼10 × 10 μm^2 free-standing membrane and 0.5 mm through-ports were exposed as individual squares backside-aligned to the microchannels. Along with cutlines, the SiN_x and underlying SiO_2 insulating layer were etched by RIE and BOE, respectively, and then opened by anisotropic etching in 33% KOH for individual 10 × 10 mm^2 chips. Figure S1 presents the full overview.

Anodic Bonding Preparation. To prepare the SiN_x surface for anodic bonding, it was first cleaned of organic contaminants in hot piranha (120 °C) for 5 min, rinsed several times in deionized water, and blown dry by nitrogen. It then underwent oxygen plasma for 5 min (0.4 mbar, ∼135 sccm, 25 W) to form a thin $SiO_2/Si_xO_yN_z$ layer. Glass slides (12 × 12 mm^2) were laser-cut from a 100 mm 150 ± 8 μm borosilicate glass wafer (Borofloat 33, Plan Optik). The glass was dipped in BOE for 15 s, cleaned in hot piranha (120 °C) for 5 min, rinsed several times in deionized water, and blown dry by nitrogen. The SiN_x surface was then brought into contact with the glass piece within a cleanroom environment and bonded using a custom-built apparatus (400 °C, 1000 V, 14 min).

PDMS Bonding. PDMS (SYLGARD 184) was mixed in a 10:1 (base:curing agent) ratio by weight, degassed, and baked on a hot plate at 80 °C for at least 5 h. Subsequently, 20 × 20 mm^2 slabs were cut and access ports were punctured through. The PDMS and SiN_x surfaces were plasma-activated in air (11 W, 515 mTorr, 50 s), brought into contact, and baked on a hot plate for 5−10 min.

Genomic DNA Labeling and Purification. Genomic DNA samples from human colorectal cancer cells (HCT116) were prepared in agarose plugs according to the IrysPrep Plug Lysis Long DNA Isolation Protocol (Bionano Genomics Inc.) with some modifications as described in the Supporting Information. Purified DNA was subsequently labeled by nick translation using nicking enzyme Nt.BspQI (NEB). Briefly, a 900 ng portion of DNA was incubated with 30 units of Nt.BspQI in 10× buffer 3.1 for 2 h. Next, 600 nM of dATP, dGTP, dCTP (Sigma), and dUTP-Atto (Jena Bioscience), 15 units of Taq polymerase, and 4.5 μL of 10x thermopol buffer was added to the nicked DNA to a final volume of 45 μL and incubated at 75 °C for 1 h. To repair the nicked DNA, 12 units of Taq ligase (NEB), 1.5 μL of 10x thermopol buffer (NEB), and 1 mM NAD+ was added to a final volume of 60 μL. Finally, the DNA was purified from excess fluorophores twice by drop dialysis using a 0.1 μm dialysis membrane (Millipore) floated on TE (10 mM Tris HCl, 1 mM EDTA, pH 8). A 0.5 μL volume of DNA was subsequently dyed at a base pair to YOYO-1 ratio of 20−25:1 in TE to a total volume of 15 μL.

Setup and Device Operation. For imaging and laser-etching, we constructed a custom-designed dual widefield/confocal microscope. In widefield mode, a 488 or 641 nm laser (iFlex-2000) was expanded to yield a ∼82 × 82 μm^2 illuminated area through a NA 1.45 100× oil objective (Olympus PlanApo). Alternatively, a ∼136 × 136 μm^2 area was obtained through a NA 1.45 60× oil objective (Olympus PlanApo). In confocal mode, a 375 nm laser (Coherent OBIS) was focused on the objective. Images were acquired on an EMCCD camera (Andor iXon 887) at 25 ms exposure and 1 × 1 binning to yield a 160 nm pixel size at 100x. Transmembrane voltages were applied using an Axopatch 200B and samples were taken at 250 kHz and filtered externally (Krohn-Hite 3202) at 10 kHz. The EMCCD camera was synchronized to the Axopatch analog acquisition *via* firepulses. DNA was pulled into the sensing region by applying vacuum (∼8−10 mbar), which could be turned on and off rapidly by electrically actuated valves (Warner). All instrumentation was controlled by custom LabVIEW software.

Loading Buffers. DNA samples were diluted in 10 mM Tris HCl pH 8 to a final concentration of 0.1−1 ng/μL. The outlet-side channel and *cis* chamber were filled with 100 mM KCl and 1 M KCl, respectively, with 10 mM Tris HCl pH 7.5 and 1 mM EDTA.

ASSOCIATED CONTENT

Supporting Information

The Supporting Information is available free of charge at https://pubs.acs.org/doi/10.1021/acsnano.9b07873.

Device fabrication overview, images of collapsed membranes, DNA combing of nick-translated DNA, additional laser drilling traces, device noise characterization, genomic DNA extraction protocol, pillar hooking and unhooking examples, translocation speed calculation, summary of tested devices, polymer extension estimation, nanopore collision events(PDF)

Movie S1: DNA stretching in pillar array (ZIP)

Movie S2: trigger mechanism used for stopping DNA (ZIP)

Movie S3: example translocation event in a 20 nm nanopore (ZIP)

Movie S4: example translocation event in a 12 nm nanopore (ZIP)

AUTHOR INFORMATION

Corresponding Author

*E-mail: ameller@technion.ac.il.

ORCID

Amit Meller: 0000-0001-7082-0985

Notes

The authors declare no competing financial interest.

ACKNOWLEDGMENTS

We thank Arik Girsault and Eran Zvuloni for their assistance in constructing the optical setup as well as Xander van Kooten for his assistance in designing the anodic bonding setup. This project has received funding from the European Research Council (ERC) under the European Union's Horizon 2020 research and innovation programme (Grant Agreement No. 833399). We also acknowledge support from the i-Core program of the Israel Science Foundation (1902/12).

REFERENCES

(1) Kidd, J. M.; Cooper, G. M.; Donahue, W. F.; Hayden, H. S.; Sampas, N.; Graves, T.; Hansen, N.; Teague, B.; Alkan, C.; Antonacci, F.; Haugen, E.; Zerr, T.; Yamada, N. A.; Tsang, P.; Newman, T. L.; Tüzün, E.; Cheng, Z.; Ebling, H. M.; Tusneem, N.; David, R.; et al. Mapping and Sequencing of Structural Variation from Eight Human Genomes. *Nature* **2008**, *453*, 56−64.

(2) Vucic, E. A.; Thu, K. L.; Williams, A. C.; Lam, W. L.; Coe, B. P. Copy Number Variations in the Human Genome and Strategies for Analysis. In *Genetic Variation Methods and Protocols*; Barnes, M., Breen, G., Eds.; Humana Press: Totowa, 2010; pp 103−117.

DOI: 10.1021/acsnano.9b07873
ACS Nano XXXX, XXX, XXX−XXX

(3) Goodwin, S.; McPherson, J. D.; McCombie, W. R. Coming of Age: Ten Years of Next-Generation Sequencing Technologies. *Nat. Rev. Genet.* **2016**, *17*, 333−351.
(4) Kaykov, A.; Taillefumier, T.; Bensimon, A.; Nurse, P. Molecular Combing of Single DNA Molecules on the 10 Megabase Scale. *Sci. Rep.* **2016**, *6*, 19636.
(5) Michalet, X.; Ekong, R.; Fougerousse, F.; Rousseaux, S.; Schurra, C.; Hornigold, N.; Van Slegtenhorst, M.; Wolfe, J.; Povey, S.; Beckmann, J. S.; Bensimon, A. Dynamic Molecular Combing: Stretching the Whole Human Genome for High-Resolution Studies. *Science* **1997**, *277*, 1518−1523.
(6) Reisner, W.; Pedersen, J. N.; Austin, R. H. DNA Confinement in Nanochannels: Physics and Biological Applications. *Rep. Prog. Phys.* **2012**, *75*, 106601.
(7) Jeffet, J.; Kobo, A.; Su, T.; Grunwald, A.; Green, O.; Nilsson, A. N.; Eisenberg, E.; Ambjornsson, T.; Westerlund, F.; Weinhold, E.; Shabat, D.; Purohit, P. K.; Ebenstein, Y. Super-Resolution Genome Mapping in Silicon Nanochannels. *ACS Nano* **2016**, *10*, 9823−9830.
(8) Gabrieli, T.; Sharim, H.; Nifker, G.; Jeffet, J.; Shahal, T.; Arielly, R.; Levi-Sakin, M.; Hoch, L.; Arbib, N.; Michaeli, Y.; Ebenstein, Y. Epigenetic Optical Mapping of 5-Hydroxymethylcytosine in Nanochannel Arrays. *ACS Nano* **2018**, *12*, 7148−7158.
(9) Nyberg, L. K.; Persson, F.; Berg, J.; Bergström, J.; Fransson, E.; Olsson, L.; Persson, M.; Stålnacke, A.; Wigenius, J.; Tegenfeldt, J. O.; Westerlund, F. A Single-Step Competitive Binding Assay for Mapping of Single DNA Molecules. *Biochem. Biophys. Res. Commun.* **2012**, *417*, 404−408.
(10) Sheats, J.; Reifenberger, J. G.; Cao, H.; Dorfman, K. D. Measurements of DNA Barcode Label Separations in Nanochannels from Time-Series Data. *Biomicrofluidics* **2015**, *9*, 1−12.
(11) Branton, D.; Deamer, D. W.; Marziali, A.; Bayley, H.; Benner, S. A.; Butler, T.; Di Ventra, M.; Garaj, S.; Hibbs, A.; Huang, X.; Jovanovich, S. B.; Krstic, P. S.; Lindsay, S.; Ling, X. S.; Mastrangelo, C. H.; Meller, A.; Oliver, J. S.; Pershin, Y. V.; Ramsey, J. M.; Riehn, R.; et al. The Potential and Challenges of Nanopore Sequencing. *Nat. Biotechnol.* **2008**, *26*, 1146−1153.
(12) Singer, A.; Rapireddy, S.; Ly, D. H.; Meller, A. Electronic Barcoding of a Viral Gene at the Single-Molecule Level. *Nano Lett.* **2012**, *12*, 1722−1728.
(13) Gilboa, T.; Torfstein, C.; Juhasz, M.; Grunwald, A.; Ebenstein, Y.; Weinhold, E.; Meller, A. Single-Molecule DNA Methylation Quantification Using Electro-Optical Sensing in Solid-State Nanopores. *ACS Nano* **2016**, *10*, 8861−8870.
(14) Kowalczyk, S. W.; Hall, A. R.; Dekker, C. Detection of Local Protein Structures along DNA Using Solid-State Nanopores. *Nano Lett.* **2010**, *10*, 324−328.
(15) Squires, A.; Atas, E.; Meller, A. Nanopore Sensing of Individual Transcription Factors Bound to DNA. *Sci. Rep.* **2015**, *5*, 11643.
(16) Venkatesan, B. M.; Bashir, R. Nanopore Sensors for Nucleic Acid Analysis. *Nat. Nanotechnol.* **2011**, *6*, 615−624.
(17) Kubota, T.; Lloyd, K.; Sakashita, N.; Minato, S.; Ishida, K.; Mitsui, T. Clog and Release, and Reverse Motions of DNA in a Nanopore. *Polymers (Basel, Switz.)* **2019**, *11*, 1−12.
(18) Ando, G.; Hyun, C.; Li, J.; Mitsui, T. Directly Observing the Motion of DNA Molecules Near Solid-State Nanopores. *ACS Nano* **2012**, *6*, 10090−10097.
(19) Muthukumar, M. Theory of Capture Rate in Polymer Translocation. *J. Chem. Phys.* **2010**, *132*, 195101.
(20) Grosberg, A. Y.; Rabin, Y. DNA Capture into a Nanopore: Interplay of Diffusion and Electrohydrodynamics. *J. Chem. Phys.* **2010**, *133*, 165102.
(21) Nelson, E. M.; Kurz, V.; Shim, J.; Timp, W.; Timp, G. Using a Nanopore for Single Molecule Detection and Single Cell Transfection. *Analyst* **2012**, *137*, 3020−3027.
(22) Jain, T.; Guerrero, R. J. S.; Aguilar, C. A.; Karnik, R. Integration of Solid-State Nanopores in Microfluidic Networks *via* Transfer Printing of Suspended Membranes. *Anal. Chem.* **2013**, *85*, 3871−3878.
(23) Tahvildari, R.; Beamish, E.; Briggs, K.; Chagnon-Lessard, S.; Sohi, A. N.; Han, S.; Watts, B.; Tabard-Cossa, V.; Godin, M. Manipulating Electrical and Fluidic Access in Integrated Nanopore-Microfluidic Arrays Using Microvalves. *Small* **2017**, *13*, 1−7.
(24) Varongchayakul, N.; Hersey, J. S.; Squires, A.; Meller, A.; Grinstaff, M. W. A Solid-State Hard Microfluidic−Nanopore Biosensor with Multilayer Fluidics and On-Chip Bioassay/Purification Chamber. *Adv. Funct. Mater.* **2018**, *28*, 1−9.
(25) Zhang, Y.; Reisner, W. Fabrication and Characterization of Nanopore-Interfaced Nanochannel Devices. *Nanotechnology* **2015**, *26*, 455301.
(26) Zhang, Y.; Liu, X.; Zhao, Y.; Yu, J. K.; Reisner, W.; Dunbar, W. B. Single Molecule DNA Resensing Using a Two-Pore Device. *Small* **2018**, *14*, 1−11.
(27) Liu, X.; Zhang, Y.; Nagel, R.; Reisner, W.; Dunbar, W. B. Controlling DNA Tug-of-War in a Dual Nanopore Device. *Small* **2019**, *15*, 1901704.
(28) Cao, H.; Tegenfeldt, J. O.; Austin, R. H.; Chou, S. Y. Gradient Nanostructures for Interfacing Microfluidics and Nanofluidics. *Appl. Phys. Lett.* **2002**, *81*, 3058−3060.
(29) Wang, C.; Bruce, R. L.; Duch, E. A.; Patel, J. V.; Smith, J. T.; Astier, Y.; Wunsch, B. H.; Meshram, S.; Galan, A.; Scerbo, C.; Pereira, M. A.; Wang, D.; Colgan, E. G.; Lin, Q.; Stolovitzky, G. Hydrodynamics of Diamond-Shaped Gradient Nanopillar Arrays for Effective DNA Translocation into Nanochannels. *ACS Nano* **2015**, *9*, 1206−1218.
(30) Puers, R.; Cozma, A. Bonding Wafers with Sodium Silicate Solution. *J. Micromech. Microeng.* **1997**, *7*, 114−117.
(31) Gu, J.; Gupta, R.; Chou, C.-F.; Wei, Q.; Zenhausern, F. A Simple Polysilsesquioxane Sealing of Nanofluidic Channels below 10 Nm at Room Temperature. *Lab Chip* **2007**, *7*, 1198−1201.
(32) Weichel, S.; De Reus, R.; Bouaidat, S.; Rasmussen, P. A.; Hansen, O.; Birkelund, K.; Dirac, H. Low-Temperature Anodic Bonding to Silicon Nitride. *Sens. Actuators, A* **2000**, *82*, 249−253.
(33) Bower, R. W.; Ismail, M. S.; Roberds, B. E. Low Temperature Si3N4 Direct Bonding. *Appl. Phys. Lett.* **1993**, *62*, 3485−3487.
(34) Shih, W. P.; Hui, C. Y.; Tien, N. C. Collapse of Microchannels during Anodic Bonding: Theory and Experiments. *J. Appl. Phys.* **2004**, *95*, 2800−2808.
(35) Kwok, H.; Briggs, K.; Tabard-Cossa, V. Nanopore Fabrication by Controlled Dielectric Breakdown. *PLoS One* **2014**, *9*, No. e92880.
(36) Tahvildari, R.; Beamish, E.; Tabard-Cossa, V.; Godin, M. Integrating Nanopore Sensors within Microfluidic Channel Arrays Using Controlled Breakdown. *Lab Chip* **2015**, *15*, 1407−1411.
(37) Carlsen, A. T.; Briggs, K.; Hall, A. R.; Tabard-Cossa, V. Solid-State Nanopore Localization by Controlled Breakdown of Selectively Thinned Membranes. *Nanotechnology* **2017**, *28*, 085304.
(38) Zrehen, A.; Gilboa, T.; Meller, A. Real-Time Visualization and Sub-Diffraction Limit Localization of Nanometer-Scale Pore Formation by Dielectric Breakdown. *Nanoscale* **2017**, *9*, 16437−16445.
(39) Gilboa, T.; Zrehen, A.; Girsault, A.; Meller, A. Optically-Monitored Nanopore Fabrication Using a Focused Laser Beam. *Sci. Rep.* **2018**, *8*, 1−10.
(40) Gilboa, T.; Zvuloni, E.; Zrehen, A.; Squires, A. H.; Meller, A. Automated, Ultra-Fast Laser-Drilling of Nanometer Scale Pores and Nanopore Arrays in Aqueous Solutions. *Adv. Funct. Mater.* **2019**, *1900642*, 1−9.
(41) Storm, A. J.; Storm, C.; Chen, J.; Zandbergen, H.; Joanny, J. F.; Dekker, C. Fast DNA Translocation through a Solid-State Nanopore. *Nano Lett.* **2005**, *5*, 1193−1197.
(42) Wanunu, M.; Morrison, W.; Rabin, Y.; Grosberg, A. Y.; Meller, A. Electrostatic Focusing of Unlabelled DNA into Nanoscale Pores Using a Salt Gradient. *Nat. Nanotechnol.* **2010**, *5*, 160−165.
(43) Doyle, P. S.; Ladoux, B.; Viovy, J. Dynamics of a Tethered Polymer in Shear Flow. *Phys. Rev. Lett.* **2000**, *84*, 4769−4772.
(44) Viero, Y.; He, Q.; Bancaud, A. Hydrodynamic Manipulation of DNA in Nanopost Arrays: Unhooking Dynamics and Size Separation. *Small* **2011**, *7*, 3508−3518.

DOI: 10.1021/acsnano.9b07873
ACS Nano XXXX, XXX, XXX−XXX

(45) McCaffrey, J.; Sibert, J.; Zhang, B.; Zhang, Y.; Hu, W.; Riethman, H.; Xiao, M. CRISPR-CAS9 D10A Nickase Target-Specific Fluorescent Labeling of Double Strand DNA for Whole Genome Mapping and Structural Variation Analysis. *Nucleic Acids Res.* **2016**, *44*, No. e11.
(46) Günther, K.; Mertig, M.; Seidel, R. Mechanical and Structural Properties of YOYO-1 Complexed DNA. *Nucleic Acids Res.* **2010**, *38*, 6526−6532.
(47) Reisner, W.; Larsen, N. B.; Silahtaroglu, A.; Kristensen, A.; Tommerup, N.; Tegenfeldt, J. O.; Flyvbjerg, H. Single-Molecule Denaturation Mapping of DNA in Nanofluidic Channels. *Proc. Natl. Acad. Sci. U. S. A.* **2010**, *107*, 13294−13299.
(48) Müller, V.; Westerlund, F. Optical DNA Mapping in Nanofluidic Devices: Principles and Applications. *Lab Chip* **2017**, *17*, 579−590.
(49) Thacker, V. V.; Ghosal, S.; Hernández-Ainsa, S.; Bell, N. A. W.; Keyser, U. F. Studying DNA Translocation in Nanocapillaries Using Single Molecule Fluorescence. *Appl. Phys. Lett.* **2012**, *101*, 223704.

DOI: 10.1021/acsnano.9b07873
ACS Nano XXXX, XXX, XXX−XXX